LAWRENCE
LIVERMORE
NATIONAL
LABORATORY

UCRL-JRNL-203446

A Modeling Approach for Burn Scar Assessment Using Natural Features and Elastic Property

Y. Zhang, D. B. Goldgof, S. Sarkar, L. V. Tsap

April 8, 2004

IEEE Transactions on Medical Imaging

Communication Submission

A Modeling Approach for Burn Scar Assessment Using Natural Features and Elastic Property

Yong Zhang, Dmitry B. Goldgof, Sudeep Sarkar, and Leonid V. Tsap*

Department of Computer Science and Engineering
University of South Florida
4202 East Fowler Ave., Tampa, FL 33620
Phone: (813) 974-2113
Fax: (813) 974-5456
zhang, or goldgof, or sarkar@csee.usf.edu

* Advanced Communications and Signal Processing Group
Electronics Engineering Department
University of California Lawrence Livermore National Laboratory
Livermore, CA 94551
tsap1@llnl.gov

Index Terms: Physical model, elastic property, burn scar, natural feature, finite element, regularization.

Abstract

[1] A modeling approach is presented for quantitative burn scar assessment. Emphases are given to: (1) constructing a finite element model from natural image features with an adaptive mesh, and (2) quantifying the Young's modulus of scars using the finite element model and the regularization method. A set of natural point features is extracted from the images of burn patients. A Delaunay triangle mesh is then generated that adapts to the point features. A 3D finite element model is built on top of the mesh with the aid of range images providing the depth information. The Young's modulus of scars is quantified with a simplified regularization functional, assuming that the knowledge of scar's geometry is available. The consistency between the Relative Elasticity Index and the physician's rating based on the Vancouver Scale (a relative scale used to rate burn scars) indicates that the proposed modeling approach has high potentials for image-based quantitative burn scar assessment.

[1]This work was performed under the auspices of the U.S. Department of Energy by University of California Lawrence Livermore National Laboratory under contract number W-7405-Eng-48. UCRL-PROC-XXXXXX

1 INTRODUCTION

Each year more than one million people suffer burn injuries in Canada and the US [14]. Accurate rating of scar condition is needed in order to design an effective treatment plan. Scar rating in clinical settings is done using the Vancouver rating scale or its variants by which experts assess the vascularity, pigmentation, pliability and size of scars [16, 22]. These rating methods suffer from their subjective nature and low consistency among rates. There is a strong need for a quantitative and objective scar rating method based on the biophysical properties of skin tissue [13].

In our previous works [20, 21, 23], we developed a comprehensive scar assessment method that utilizes the color, texture, pliability, thickness and size of scars. In this paper, we advance a physical model-based scar rating method which focuses on estimating the relative elasticity of scars. The contributions of the proposed method are: (1) noninvasive natural image features are used to generate an adaptive mesh and to build a finite element model. In previous works, we had used artificial markers (ink stamps) on the skin to facilitate model construction. The use of natural features enables us to quantify the elastic property without the need of any markers, and hence greatly enhances the applicability of the proposed rating method; (2) a robust procedure of quantifying the scar elasticity is established using the regularization method so that the noisy data can be handled properly.

Although effort has been made to measure the scar elasticity directly using contact devices [1], there is need for noninvasive methods that infer scar elasticity from the observed tissue motion. Both ultrasonic and MR images have been used in tissue property reconstruction. Ultrasonic wave can penetrate soft tissues and is suitable for the study of internal organs [18, 11, 12]. But ultrasonic images are plagued by the noise artifacts and low resolution. MRI elastography has the advantage that motion can be measured with high resolution [10]. Creswell *et al* [3] used the MRI tagging technique and iterative finite element method for heart model evaluation. But MR imaging is expensive and less flexible. We will use regular optical and range images to quantify scar elasticity.

Two important issues in scar elasticity estimation are the ill-posedness and the computational cost. The stability of inverse solution can be partially restored through the regularization methods such as the Tikhonov functional. To reduce the computational complexity, we experimented with the following approaches in the context of burn scar assessment: (1) reduce the parameter space by posing stronger constraints; (2) reduce the parameter space by using an adaptive finite element mesh.

2 MODEL CONSTRUCTION

Governing Equations The mechanical behavior of skin is determined by the presence of collagen fibers, elastin fibers and lubricating ground substance [9, 6, 19]. Burn scars tend to have random organization of collagen fibers during tissue regeneration. We assume that the mechanical behavior of burn scars can be approximated by an elastic and isotropic model. Let $\mathbf{u}$ be the displacement vector, $[e] = [e_{ij}, \gamma_{ij}]$ be the strain tensor, $[\sigma] = [\sigma_{ij}, \tau_{ij}]$ be the stress tensor, ρ_0 be the mass density, $\mathbf{B}$ be the body force, and E and ν be the Young's modulus and the Poisson's ratio. The governing equation of elastic body motion can be obtained from three basic equations: (1) the strain compatibility equation, (2) the motion equation (conservation of momentum), and (3) the constitutive equation.

The strain compatibility equation is the necessary and sufficient condition to ensure that the strain components give a single-valued continuous displacement:

$$\nabla \times (\nabla \times e)^T = 0. \tag{1}$$

The principle of conservation states that the rate of change of the total linear momentum of a continuous medium equals the sum of all the external forces:

$$\rho_0 \frac{\partial^2 \mathbf{u}}{\partial t^2} = \nabla \cdot \sigma + \mathbf{B}. \tag{2}$$

The constitutive equation for linear and isotropic materials is:

$$\begin{bmatrix} \sigma_{xx} \\ \sigma_{yy} \\ \sigma_{zz} \\ \tau_{xy} \\ \tau_{yz} \\ \tau_{zy} \end{bmatrix} = \frac{E}{(1+\nu)(1-2\nu)} \begin{bmatrix} 1-\nu & \nu & \nu & 0 & 0 & 0 \\ \nu & 1-\nu & \nu & 0 & 0 & 0 \\ \nu & \nu & 1-\nu & 0 & 0 & 0 \\ 0 & 0 & 0 & \frac{1}{2}-\nu & 0 & 0 \\ 0 & 0 & 0 & 0 & \frac{1}{2}-\nu & 0 \\ 0 & 0 & 0 & 0 & 0 & \frac{1}{2}-\nu \end{bmatrix} \begin{bmatrix} e_{xx} \\ e_{yy} \\ e_{zz} \\ \gamma_{xy} \\ \gamma_{yz} \\ \gamma_{zy} \end{bmatrix}. \tag{3}$$

Combining equations (1), (2), and (3), we have the governing equation for elastic deformation:

$$\rho_0 \frac{\partial^2 \mathbf{u}}{\partial t^2} = \nabla \cdot [\lambda(\nabla \cdot \mathbf{u})\mathbf{I} + G\nabla\mathbf{u} + G(\nabla\mathbf{u})^T] + \mathbf{B}, \tag{4}$$

where G and λ are the Lamé constants, which can be computed from E and ν:

$$G = \frac{E}{2(1+\nu)}, \quad \lambda = \frac{\nu E}{(1+\nu)(1-2\nu)}. \tag{5}$$

Extraction of Natural Point Features We use the Shi-Tomasi detector to extract salient points in scar images [17, 15]. For each pixel p in the image, we compute a 2×2 matrix (g) within a window (w):

$$g = \begin{bmatrix} \sum^w \frac{\partial I}{\partial x}\frac{\partial I}{\partial x} & \sum^w \frac{\partial I}{\partial x}\frac{\partial I}{\partial y} \\ \sum^w \frac{\partial I}{\partial y}\frac{\partial I}{\partial x} & \sum^w \frac{\partial I}{\partial y}\frac{\partial I}{\partial y} \end{bmatrix} \tag{6}$$

where I is the image intensity and (x, y) represent row and column. We compute the first derivatives by convolving the intensity with the derivative of Gaussian filter (G): $\frac{\partial I}{\partial x} = \frac{\partial G}{\partial x} * I, \quad \frac{\partial I}{\partial y} = \frac{\partial G}{\partial y} * I$. We then compute the coefficients of gradient matrix: $\frac{\partial I}{\partial x}\frac{\partial I}{\partial x}$, $\frac{\partial I}{\partial y}\frac{\partial I}{\partial y}$, $\frac{\partial I}{\partial x}\frac{\partial I}{\partial y}$, $\frac{\partial I}{\partial y}\frac{\partial I}{\partial x}$. We sum up the coefficients of all pixels inside w to produce the matrix g of pixel p. We then compute the eigenvalues of matrix g: $(\lambda 1, \lambda 2)$. Given a threshold T, satisfaction of the condition: $\min(\lambda 1, \lambda 2) > T$, indicates that the window contains a corner/point with two strong edges along the eigenvector directions. The choice of T value depends on the size and quality of images, as well as the number of features desired. If T is set too high, only a small number of features can be extracted. We used a value of $T = 1$ for all of the scar experiments. With this value, 400-800 features can be ensured in the scar images, which suffices the need of building a relatively dense finite element mesh.

We use another threshold h, the minimum distance between two adjacent points, to control feature distribution. Since scars have lower intensity than normal skins, we change the value of h adaptively based on the intensity variation. We first select an area that contains only scars and skins. We then equalize the selected area to highlight the intensity contrast between scars and skins. For each feature point, its h is computed based on the average intensity in w, scaled linearly by the overall intensity variation in the modeling area: $h = H_{min} + (I_w - I_{min})\frac{H_{max} - H_{min}}{I_{max} - I_{min}}$, where h is the minimum distance between a feature and its neighbors, I_w is the average intensity in w, (I_{max}, I_{min}) are the maximum and minimum intensities in modeling area after equalization, and (H_{max}, H_{min}) are user-specified maximum and minimum h that correspond to (I_{max}, I_{min}). Features in scars tend to have smaller h than features in normal skins. After computing h for each feature, we sort all features based on the number of their neighbors that are in conflict with their h value. By "conflict" we mean that the distance between a feature and its neighbors is less than its h. We then iteratively remove the feature that has the most conflicts until no conflict exists. The final distribution has more features in scars than in skins.

All scar images have the resolution of 640×480 pixels. Features are extracted using a window size of 9×9. If the window size is too small (3×3), the window will not contain enough information and certain features will be missed. If the window size is too large (15×15), it will cause strong overlap between adjacent features. So the window size of 9×9 is a compromise that also depends upon the image size and resolution. The minimum distance (H_{min}) is in the range of 15-20 pixels, and H_{max} is set to be 1.3 - 2.5 times larger than H_{min}. The choice of H_{min} depends on the size of scar studied. If H_{min} is too

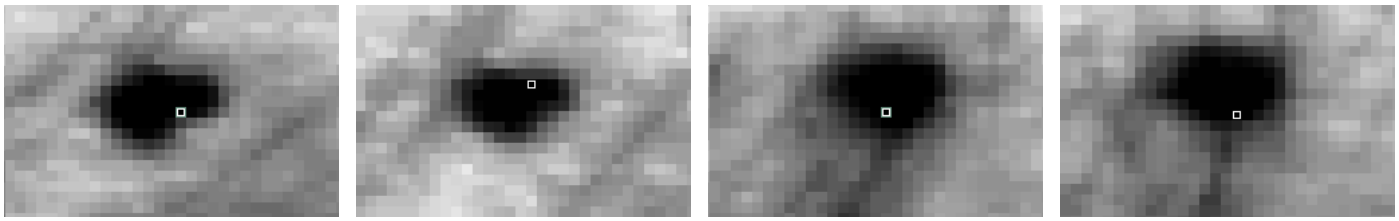

(a) Feature in frame 1 (b) Corresp. in frame 2 (c) Feature in frame 1 (d) Corresp. in frame 2

Figure 1: Position shift between the corresponding features in two frames. Note that features in (a,b) and (c,d) are corresponding pairs. The white square indicates the computed feature position by the feature detector. The shift between (a) and (b) is 3 pixels. The shift between (c) and (d) is 2 pixels.

Table 1: The performance of point feature detector with burn scar images

	Min.	Max.	Average
feature position shift (pixel)	0	4.5	2.1
actual displacement (pixel)	11.9	36.2	24.8
error (shift/displacement)	0.0%	13.3%	7.2%

large, there may not be enough features in scar areas and vise versa. The same argument applies to the choice of H_{max}. Those heuristic parameters must be tuned for a specific setting depending upon the size and quality of images and the size of scars.

To quantify the precision of feature extraction, we examined 218 corresponding feature pairs extracted from scar images. For each patient, two frames were taken (before and after deformation). Features were then extracted from two frames. There exist small shifts between the computed positions of corresponding features in two frames. Two typical feature pairs are shown in Figure 1. The white square indicates the computed position by the feature detector. The first correspondence (a,b) has a shift of 3 pixels, and the second correspondence (c,d) has a shift of 2 pixels. Note that the intensity pattern of features changed slightly between two frames due to the variations in lighting condition, projection and skin deformation. The actual displacements due to skin deformation between two correspondences are 26 and 21 pixels. Since we are interested in obtaining good displacement data for scar modeling, we define the extraction error as the ratio of the computed position shift to the actual displacement. For the two feature pairs shown in Figure 1, the extraction errors are 11.5% and 9.5%, respectively. For 218 feature pairs we examined, the results are summarized in Table 1. With current imaging setting and feature extraction method, the average error introduced in feature extraction is less than 10%.

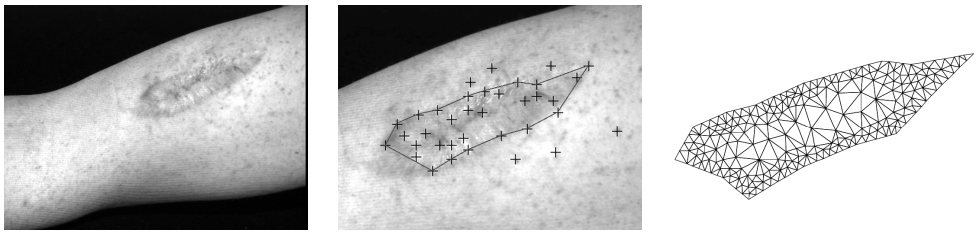

(a) (b) (c)

Figure 2: Adaptive meshing using point features. (a) Scar image. (b) Point features and ROI. (c) Adaptive triangle mesh with refinement at the boundary.

Adaptive Meshing Given a set of points distributed on object's surface, we can generate an adaptive mesh based on the Delaunay principle [2], which states that no vertex is allowed inside the circumscribing circle of any element. We use the following meshing procedure: (1) extract point features from images; (2) select the points inside the region of interest (ROI) for which a physical model will be built; (3) link the points on the boundary of ROI to form a closed polygon or surface; (4) generate an adaptive Delaunay mesh using feature points as its nodes; (5) refine the mesh.

An algorithm simply obeying the Delaunay principle yields a mesh that adapts to the feature set without the guarantee of mesh quality. Refinement must be performed to insert new nodes into the area of interest as a quality assurance procedure. We follow these guidelines in the node insertion: (1) new nodes are added at the region of high curvature to ensure accurate surface representation; (2) new nodes should subdivide the thin element into regular elements to reduce modeling errors; (3) new nodes are added at regions of property discontinuities which could cause large modeling errors. Figure 2 shows an example of adaptive triangle mesh.

3 ESTIMATE SCAR ELASTICITY

Range Scanner Setting A range scanner is used to obtain 3D information of features and the displacement between corresponding feature pairs. The setting of K2T range scanner is illustrated in Figure 3 (a). Range camera acquires a raster of depth measurements of object and records the image over a quantified range. The K2T system consists of a CCD camera and a structured light projector, and computes the depth from images of striped light patterns. An example of structured light patterns is shown in Figure 3 (b). In scar study, the effective imaging area is about 30-35 cm cube. The distance between patients and the range camera is about 100-130 cm.

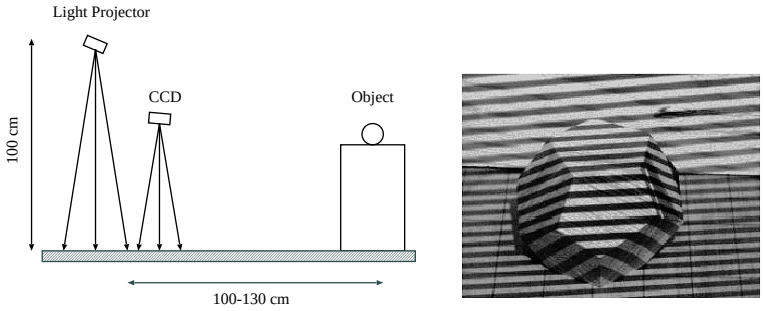

(a) K2T imaging geometry (b) Light stripe pattern

Figure 3: The geometry of K2T range scanner for burn scar study.

A set of images (2-4 frames) was taken while patient's skin was stretched. Since the scar condition of most patients did not allow the use of contact devices, patient's skin was pulled gently by hands to avoid pain and further damage. Therefore, it was not possible to measure the forces applied to patient's skin. 3D displacement ($\mathbf{u}$) obtained from intensity and range images is used to compute the objective function in an "output-least-squared" form: $\|F(E) - \mathbf{u}\|^2$, where $F(E)$ denotes the forward model.

Regularization and Assumptions We use a Poisson's ratio of 0.495 by approximating the skin tissue as near-incompressible material. We consider the governing equation of static case:

$$\nabla \cdot [\lambda(\nabla \cdot \mathbf{u})\mathbf{I} + G\nabla\mathbf{u} + G(\nabla\mathbf{u})^T] + \mathbf{B} = 0, \tag{7}$$

and define a differential operator $A(E)$ as:

$$A(E) = \nabla \cdot [\lambda(\nabla \cdot (\cdot))\mathbf{I} + G\nabla(\cdot) + G(\nabla(\cdot))^T]. \tag{8}$$

Using $A(E)$, we obtain a nonlinear operator equation:

$$F(E) = -\mathbf{B}A(E)^{-1} = \mathbf{u}. \tag{9}$$

We assume that the nonlinear operator $F : X \rightarrow Y$ is continuously Fréchet differentiable and X and Y are the Hilbert spaces. This inverse operator equation is likely ill-posed. Because of the discontinuous dependence of solution (E) on noisy data ($\mathbf{u}$), the solution obtained by minimizing the "output-least-squared" objective function is numerically unstable and certain forms of regularization must be imposed [5]. We use the Tikhonov functional in its variational form:

$$T(E) = \|F(E) - \mathbf{u}\|^2 + \alpha\|W(E - E^*)\|^2, \tag{10}$$

where E^* denotes the prior knowledge of the inverse solution, α is the regularization parameter and W is the smoothness matrix. The difficulty of minimizing the Tikhonov functional of nonlinear equations is that the convexity can only be guaranteed locally. The gradient methods can be used to find the

minimizer of the Tikhonov functional, provided that they start with a good initial guess. Applications of the Tikhonov functional to elasticity reconstruction of soft tissues have been reported in [8, 4].

We are interested in determining the *relative* elasticity of scars. We can obtain good information about the geometry of scars from image cues (intensity, color and texture). To reduce the computational complexity, we make several assumptions: (1) the geometry of scars is known; (2) the elasticity of scar is higher than that of normal skin; (3) the elasticity of background normal skin is known. We then transform the minimization of (10) into a one-dimensional search problem with two steps:

1. Determine the regularization parameter using the L-curve method [7].
2. Change the elasticity of scars (E_s) until the minimizer of the simplified functional is found:

$$T(E_s) = \|F(E_s) - \mathbf{u}\|^2 + \alpha \|W(E_s - E_s^*)\|^2. \tag{11}$$

We use the L-curve method to choose the regularization parameter. The log of the regularized solution norm $log||E||$ is plotted against the log of the residual norm $log||F(E) - \mathbf{u}||$ for a range of α. The optimal α is chosen to be the one that corresponds to the corner of the L-curve. The intuitive interpretation of the L-curve method is that the solution norm will go to the maximum and the residual norm will go to the minimum as α approaches zero, and vice versa.

Boundary Condition Specification We specify displacements at the boundary nodes that are also feature points. We then interpolate displacements for the boundary nodes that were added during mesh refinement. We designate the feature points inside the modeling domain as the controlling nodes, on which the measured displacements and the simulated displacements by forward model are used to calculate the residual norm. In inverse problems, the measured force helps find a unique inverse solution. Since in our case only displacement is available, we use the elasticity of normal skins as a reference to determine the relative elasticity of scars. The reported Young's modulus values of soft tissues are in the range of 1-100 kPa [6, 19]. In scar assessment, we used a Young's modulus of 5 kPa for normal skin.

It is worth noting that the body force ($\mathbf{B}$) in (7) and (9) should not be confused with the boundary conditions in normal sense such as surface force/traction. The variation of body force (mainly gravity or electromagnetic field) is a significant factor in the simulation of large-sized objects such as the sea water in a bay or the planet earth. But for small objects such as scars, body force can be treated as a constant. In the "output-least-squared" formulation of inverse problem, the body force in the forward

Table 2: The estimated relative scar elasticity (kPa)

Patients	Scar elasticity (Natural features)	Scar elasticity (Artificial markers)	Absolute error	Relative error
scar-970407	53	46	7	13.2%
scar-970416	12	14	2	16.6%
scar-970425	41	37	4	9.7%
scar-970922	19	18	1	5.3%

Errors are computed between the results using natural features and artificial markers. The elasticity of normal skin used in experiments is 5 kPa.

model ($F(E)$) does not show up explicitly. The algorithm that minimizes $T(E)$ does not need to know what kind of body force is used in the forward modeling.

4 EXPERIMENTS

Data Set The data set includes images of four patients that were taken at different healing stages. The boundaries between scars and normal skins can be clearly identified in those images. To determine to what degree the accuracy of estimated Young's modulus will be affected by the use of natural features, we experimented with both artificial markers and natural features.

Quantify Scar Elasticity We carried out two independent experiments, one using artificial markers and one using natural features, to determine if the natural feature is a viable option for replacing the artificial marker. The results for all patients are listed in Table 2. Although direct measurements of scar's Young's modulus are not available for those patients, the fact that the differences between the estimated Young's modulus using artificial markers and using natural features are very small suggests a high level of consistency. The results of patient-970922 are plotted in Figure 4. As expected, experiment using artificial markers shows a slightly better performance than that using natural features, as indicated by the minimization curves (Figure 4 (f)). But the disparity between two curves is very small. More importantly, the minimum points of two curves are almost identical (18 kPa and 19 kPa). The strain distributions also match well with scar distribution.

The errors in measured displacements mainly came from two sources: (1) feature extraction errors caused by illumination and texture variations; (2) correspondence errors. Since we manually established the correspondence, the disparity between the modeling results of using natural features and using

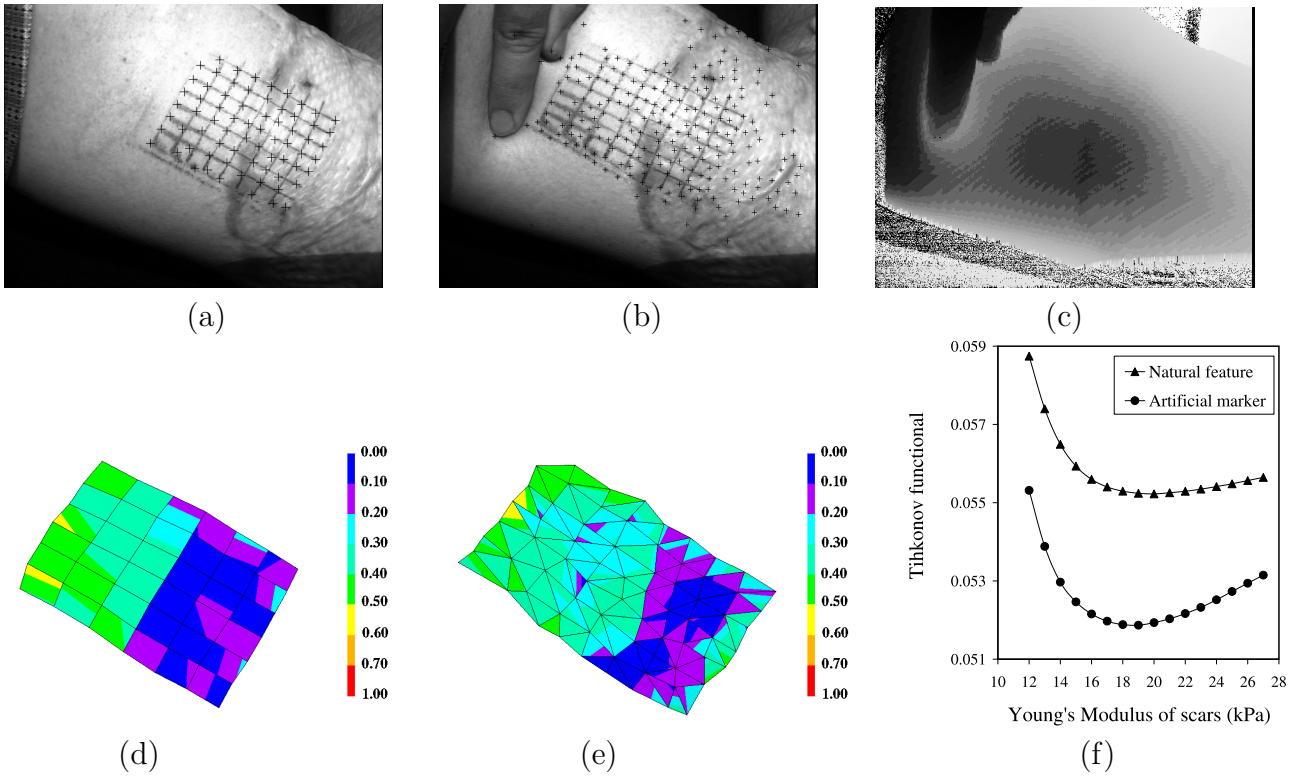

Figure 4: Estimated elasticity and strain (patient-970922). (a) Scar image. (b) After being stretched. (c) Range image. (d) Strain using marker. (e) Strain using natural features. (f) Minimization curves.

artificial markers is mainly caused by the feature extraction error. As analyzed in Section 2, the feature extraction error is less than 10% on average, which is an acceptable value for burn scar assessment.

Relative Elastic Index Current clinical scar assessment methods are based on a relative rating scale. We want to investigate if there exists a positive correlation between the clinical rating and the estimated elasticity ratio of scars to normal skins, so that we can establish a standard that is quantitative and comparable to the one used by physicians. We define the Relative Elastic Index (REI) as the ratio of average Young's modulus of scars to that of normal skins:

$$REI = \frac{\sum_{i=1}^{n} E_i/n}{\sum_{j=1}^{m} E_j/m}, \tag{12}$$

where n and m are the numbers of elements inside scars and normal skins, respectively.

In Table 3, we list physician's ratings based on the relative rating scale, as well as REIs using both artificial markers and natural features. In all experiments, patient's skin was stretched along two directions (horizontal and vertical). So, each patient was studied twice. In Figure 5, the REIs using natural features and artificial markers are plotted against the physician's ratings. Two important

Table 3: Comparison of physician's rating and Relative Elastic Index (REI)

	Physician's rating	REI using natural features	REI using artificial markers
scar-970407(hori)	4.5	9.5	8.0
scar-970407(vert)	4.5	9.1	7.3
scar-970416(hori)	3.0	2.8	3.3
scar-970416(vert)	3.0	4.1	3.8
scar-970425(hori)	3.3	6.3	5.0
scar-970425(vert)	3.3	7.4	5.6
scar-970922(hori)	2.0	2.2	2.3
scar-970922(vert)	2.0	2.8	2.0
normal-skin(hori)	1.0	1.0	1.0
normal-skin(vert)	1.0	1.0	1.0

For each patient, the skin was stretched in two directions, horizontally and vertically. The REI of normal skin (1.0) is defined as the baseline.

observations can be made: (1) there exists a good correlation between the physician's ratings and the REIs using either natural features or artificial markers; (2) the REIs computed using natural feature are consistent with those using artificial markers, especially for less damaged burn scars. The slight deviation from the linear monotonic relationship is probably caused by the complex scar patterns, which affect both feature extraction and matching. This problem can be solved by calibrating the model against the ground truth obtained from direct property measurement, a possibility that is currently under investigation. It should be pointed out that, due to the limited number of patients being studied, we do not draw any statistical conclusion at this point about the correlation between the physicians' rating and the REI.

5 CONCLUSIONS

We present a modeling approach for quantitative burn scar assessment. We construct a finite element model using a Delaunay mesh that is adapted to natural image features. The use of natural features and adaptive mesh not only increases the computational efficiency, but also allows us to work with scar images without the need of tagging artificial markers. We find that the difference between the modeling results of using artificial markers and using natural features is negligible, indicating that natural feature is a viable option for conducting quantitative burn scar assessment. We quantify burn scar damage by estimating its Young's modulus using a simplified regularization method. Experiments show that the proposed method is robust when presented with noisy data. The positive correlation between the

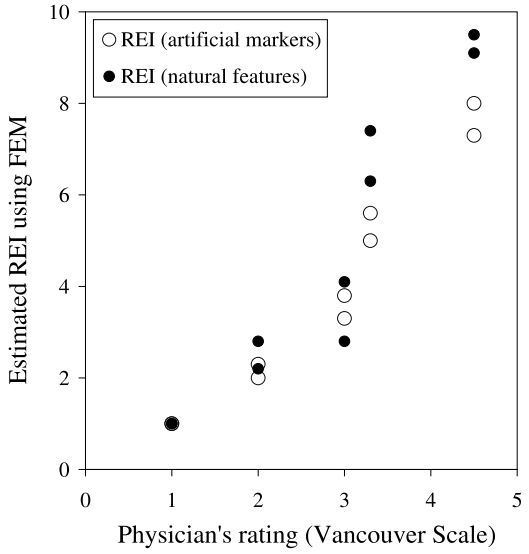

Figure 5: Correlation between physician's rating and REIs using natural features and artificial markers.

physician's rating and the REI (using both natural features and artificial markers) suggests that the proposed modeling approach can provide a quantitative and objective evaluation of burn scar damage.

It should be stressed that, although the linear model is widely used in physics-based simulations, including the burn scar assessment, the biomechanical behavior of soft tissues is intrinsically nonlinear. We choose the linear model for this study based on the assumption that the deformation of scar/skin is relatively small so that it can be approximated by a linear model. In future investigations, we will revisit the nonlinear aspect of burn scar modeling, both geometrically (Green strain tensor) and materially (viscoelastic and plastic materials), to further quantify the impact of linearity assumption on burn scar assessment.

References

[1] T. H. Bartell, W. W. Monafo, and T. A. Mustoe, "A new instrument for serial measurement of elasticity in hypertropic scar," *Journal of Burn Care and Rehabilitation*, vol. 9, pp. 657-660, 1988.

[2] G. F. Carey, *Computational Grids : Generation, Adaptation, and Solution Strategies.* Series in Computational and Physical Processes in Mechanics and Thermal Science. Taylor & Francis, 1997.

[3] L. L. Creswell, M. J. Moulton, S. G. Wyers, J. S. Pirolo, D. S. Fishman, W. H. Perman, K. W. Myers, R. L. Actis, M. W. Vannier, B. A. Szabo, and M. K. Pasque, "An experimental method for evaluating constitutive models of myocardium in in vivo hearts," *American Journal of Physiology, Heart and Circulatory Physiology*, vol. 267, pp. 853-863, 1994.

[4] M. M. Doyley, P. M. Meaney, and J. C. Bamber, "Evaluation of an iterative reconstruction method for quantitative elastography," *IEEE Phys. Med. Biol.*, vol. 45, pp. 1521-1540, 2000.

[5] H. W. Engl, M. Hanke, and A. Neubauer, *Regularization of Inverse Problems*, Kluwer Academic Publishers, c1996.

[6] Y. C. Fung, *Biomechanics; Mechanical Properties of Living Tissues*, Springer-Verlag, 2nd ed. 1993.

[7] P. C. Hansen, "Analysis of discrete ill-posed problems by means of the L-curve," *SIAM Rev.*, vol. 34, pp. 561-580, 1992.

[8] F. Kallel and M. Bertrand, "Tissue elasticity reconstruction using linear perturbation method," *IEEE Trans. Med. Imag.*, vol. 15, no. 3, pp. 299-313, 1996.

[9] W. F. Larrabee and J. A. Galt, "A finite element model of skin deformation. (iii) the finite element model," *Laryngoscope* , vol. 96, pp. 413-419, 1986.

[10] R. Muthupillai, D. J. Lomas, P. J. Rossman, J. F. Greenleaf, A. Manduca, and R. L. Ehman, "Magnetic resonance elastography by direct visualization of propagating acoustic strain waves," *Science*, vol. 269, pp. 1854-1857, 1995.

[11] J. Ophir, I. Cespedes, H. Ponnekanti, Y. Yazdi, and X. Li, "Elastography: A quantitative method for measuring the elasticity of biological tissues," *Ultrasonic Imaging*, vol. 13, pp. 111-134, 1991.

[12] K. J. Parker, L. Gao, R. M. Lerner, and S. F. Levinson, "Techniques for elastic imaging: a review," *IEEE Engineering in Medicine and Biology*, vol. 15, pp. 52-59, 1996.

[13] P. S. Powers, S. Sarkar, D. B. Goldgof, C. W. Cruse, and L. V. Tsap, "Scar Assessment: Current problems and future solutions," *Journal of Burn Care and Rehabilitation*, vol. 20, no. 1, Jan. 1999.

[14] J. R. Saffle, B. Davis, and P. Williams, "Recent outcomes in the treatment of burn injury in the United States: A report from the American Burn Association Patient Registry," *Journal of Burn Care and Rehabilitation*, vol. 16, pp. 219-232, May 1995.

[15] C. Schmid, R. Mohr, and C. Bauckhage, "Evaluation of interest point detectors," *International Journal of Computer Vision*, vol. 37, no. 2, pp. 151-172, 2000.

[16] T. Sullivan, J. Smith, J. Kermode, E. McIver, and D. J. Courtemanche, "Rating the burn scar," *Journal of Burn Care Rehabilatation*, vol. 11, pp. 256-260, 1990.

[17] J. Shi and C. Tomasi, "Good features to track," *IEEE Conference on Computer Vision and Pattern Recognition (CVPR), Seattle*, pp. 593-600, June 1994.

[18] A. R. Skovoroda, S. Y. Emelianov, M. A. Lubinski, A. P. Sarvazyan, and M. O'Donnell, "Theoretical analysis and verification of ultrasound displacement and strain imaging," *IEEE Trans. Ultrasonics, Ferroelectrics, and Frequency Control*, vol. 41, no. 3, pp. 302-313, 1994.

[19] J. G. Thacker, "The elastic properties of human skin *in vivo*," Ph.D. Dissertation, University of Virginia, Charlottesville, VA, 1976.

[20] L. V. Tsap, D. B. Goldgof, S. Sarkar, and P. S. Powers, "A vision-based technique for objective assessment of burn scars," *IEEE Trans. Med. Imag.*, vol. 17, no. 4, pp. 620-633, 1998.

[21] L. V. Tsap, D. B. Goldgof, and S. Sarkar, "Nonrigid motion analysis based on dynamic refinement of finite element models," *IEEE Trans. Pattern Analysis and Machine Intelligence*, vol. 22, no. 5, pp. 526-543, 2000.

[22] E. K. Yeong, R. Mann, L. H. Engrav, M. Goldberg, V. Cain, B. Costa, M. Moore, D. Nakamura, J. Lee, "Improved burn scar assessment with use of a new scar-rating scale," *Journal of Burn Care and Rehabilitation*, vol. 18, no. 4, pp. 353-355, 1997.

[23] Y. Zhang, D. B. Goldgof, S. Sarkar, and L. V. Tsap, "Model-based nonrigid motion analysis using natural feature adaptive mesh," *Proceedings of International Conference on Pattern Recognition*, pp. 839-843, 2000.